



Application of dual-anneal diffusion multiples to the effective study of phase diagrams and phase transformations in the Fe–Cr–Ni system

Siwei Cao and Ji-Cheng Zhao*

Department of Materials Science and Engineering, The Ohio State University, OH, USA

Received 21 September 2014; revised 28 November 2014; accepted 9 December 2014

Available online 11 February 2015

Abstract—A dual-anneal diffusion multiple (DADM) approach is developed for effective determination of intermediate-temperature phase diagrams that are critical to the establishment of reliable thermodynamic databases. A large amount of phase equilibrium data was obtained from DADMs to construct the Fe–Cr–Ni isothermal sections at 1200, 900, 800 and 700 °C. The DADM approach is also a systematic and effective way to study phase precipitation from wide ranges of compositions, thus generating rich atlases of microstructures induced by various transformations. The results from this study indicate that the body-centered cubic to sigma phase transformation in the Fe–Cr–Ni system took place initially through a massive transformation mechanism.

© 2014 Acta Materialia Inc. Published by Elsevier Ltd. All rights reserved.

Keywords: Fe–Cr–Ni; Phase diagrams; Phase transformation; Massive transformation; Diffusion multiple

1. Introduction

Most structural materials are used at or below intermediate temperatures during long-term service. The intermediate temperatures are defined here as around half of the homologous melting temperature (in kelvin). Due to the slow diffusion kinetics and thus the long annealing durations required to reach thermodynamic equilibrium, studies on phase diagrams at intermediate temperatures are not widely performed, resulting in a severe worldwide shortage of such phase diagrams. This shortage affects the reliability of thermodynamic modeling and the design of alloys, since most of the thermodynamic assessments were made using phase equilibrium data obtained mostly at high temperatures. When there are a lot of experimental data at relatively high temperatures and only limited (or often no) data at intermediate temperatures, the fitted thermodynamic parameters closely represent the experimental results of high temperatures, but describe the phase equilibria at intermediate and low temperatures poorly (see [Supplementary Information for more detail](#)). Extrapolation of the high-temperature assessments to intermediate temperatures can lead to large uncertainty in thermodynamic predictions at intermediate temperatures and below. Thus, it is significant to provide experimental phase diagrams at intermediate temperatures to improve the thermodynamic

parameters in CALPHAD modeling for more reliable predictions at long-term-use temperatures.

A dual-anneal diffusion multiple (DADM) approach is tested in the current study to extend the applicability of the diffusion-multiple methodology [1–4] to the effective phase diagram determination at intermediate temperatures and to study phase transformations. The Fe–Cr–Ni system is selected as the test bed for this study because it has more prior experimental data that can be used to check the reliability of the results obtained from DADMs. In addition, the Fe–Cr–Ni phase equilibria and phase transformation kinetics are very important for the design of new generations of steels and for understanding the behavior of existing steels at their service temperatures. For the Fe–Cr–Ni system, the intermediate temperatures are around 600–900 °C.

The basic idea of the DADM approach is to first anneal diffusion multiples at a high temperature to quickly form, thanks to relatively fast diffusion, solid solutions and intermetallic compounds. A subsequent anneal of the diffusion multiples at an intermediate temperature would induce phase precipitation from the supersaturated solid solutions and thus allow the determination of phase equilibria, as well as the study of phase transformations across wide compositions at the temperature of interest. In a certain sense, the first diffusion anneal is equivalent to making many compositions and the second heat treatment is equivalent to annealing at a temperature of interest for individually made alloys. In this regard, the temperatures accessible to the individual alloy method for phase diagram determination should also be suitable for the DADM approach. The

*Corresponding author. Tel.: +1 614 292 9462; e-mail: zhao.199@osu.edu

successful use of DADMs may help to significantly enrich the phase diagram literature at intermediate temperatures. The DADM method can avoid the time and cost of making many individual alloys, and can provide much more systematic investigations due to the continuous variations of composition in single-phase regions formed during the high-temperature annealing. It also circumvents the slow diffusion kinetics and shallow diffusion zones that would occur if a diffusion multiple is only annealed at an intermediate temperature (without the high-temperature anneal). In addition, DADMs offer an amazing diversity of precipitate microstructures and contain rich information on phase transformations. This DADM approach was tested on the Fe–Cr–Ni system at 1200, 900, 800 and 700 °C through comparison of the current experimental measurements with Thermo-Calc simulations as well as prior experimental results. A diverse atlas of microstructures induced by various phase transformations is also obtained.

Bain and Griffiths [5] were the first to report the existence of the sigma (σ) phase in the Fe–Cr–Ni ternary system, and they also defined relative positions of gamma (face-centered cubic (fcc), γ) and alpha (body-centered cubic (bcc), α) phases on the iron-rich side. Wever and Jellinghaus [6] confirmed the existence of σ and studied the Fe–Cr–Ni system above 1100 °C to construct the liquidus surface. Subsequently, Schultz and Merrick [7], Hasebe and Nishizawa [8], Schurmann and Brauckmann [9], Mundt and Hoffmeister [10], Sopousek and Vrestal [11], Sopousek and Kruml [12] and Hertzman and Sundman [13] studied phase equilibria in the Fe–Cr–Ni system at intermediate temperatures. The new results from DADMs will be compared with those prior experimental results and thermodynamic calculations in Section 3.

2. Experimental procedure

Two Fe–Cr–Ni–Co–Mo diffusion multiples of identical geometry were made, as shown in Fig. 1. In addition to the system of interest (Fe–Cr–Ni), there are seven other ternary systems/trijunctions in the diffusion multiples: Co–Cr–Fe, Co–Cr–Mo, Co–Fe–Ni, Co–Mo–Ni, Cr–Fe–Mo, Cr–Mo–Ni and Fe–Mo–Ni. The results for these ternary systems will be obtained and reported separately, since each trijunction provides enormous amounts of information on precipitation and phase equilibria.

The diffusion multiples were made by assembling finely polished pure Fe (99.8%), Co (99.9%), Cr (99.9%) and Mo (99.95%) metal pieces together in a pure Ni (99.9%) cylinder with a 19 × 25 mm rectangular opening along the cylindrical axis. The height of the Ni cartridges is 38 mm. The diffusion multiple dimensions are shown in Fig. 1e. Each diffusion multiple employed two Mo bars and one Cr bar of 6.3 × 6.3 × 38 mm, as well as one Mo plate, two Fe plates, two Co plates and one Cr plate of 9.5 × 6.3 × 38 mm. All the pure metal pieces were cut into shapes using electrodischarge machining (EDM). Two Ni cap plates were put on the top and bottom of each Ni cartridge, with the pure metal pieces assembled inside before electron-beam welding in a vacuum chamber along the edges of the Ni cartridge and the Ni caps. Hot isostatic pressing (HIP) was performed at 1200 °C for 8 h under 207 MPa argon pressure to achieve good interfacial contacts between the metal pieces. After cooling down to room

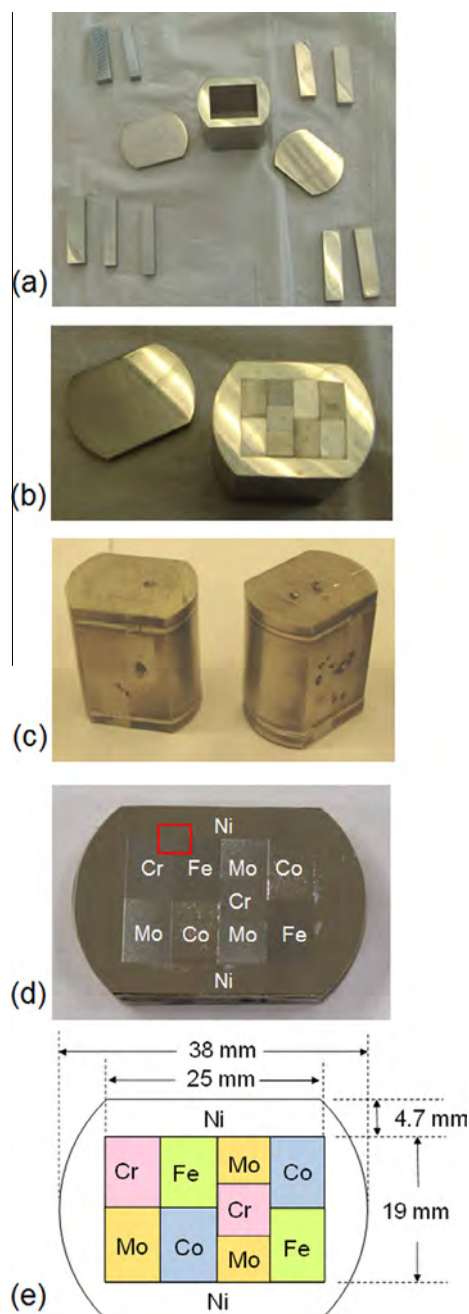


Fig. 1. Diffusion multiple fabrication: (a) components before assembling; (b) metal pieces put together to show their arrangement; (c) samples after electron beam welding but before HIP treatment; (d) an EDM-cut sample slice parallel to the Ni cap after heat treatment; and (e) exact cross-section dimensions of the diffusion multiples. All the results reported herein were obtained from the Fe–Cr–Ni trijunction area marked by a red square in (d). (For interpretation of the references to colour in this figure legend, the reader is referred to the web version of this article.)

temperature inside the HIP unit, the samples were encapsulated individually in two separate sealed quartz tubes filled with argon to reduce possible oxidation during diffusion heat treatment. A small Ta piece wrapped in Ti foil was placed inside each quartz tube next to the sample (without contact) to help absorb any oxygen diffusing through the quartz tube.

After annealing at 1200 °C for 500 h and water quenching to ambient temperature (by breaking the quartz tube), one diffusion multiple was then cut into ~6 mm thick slices (parallel to the Ni caps) using EDM, before being subjected to the regular metallographic sample preparation procedures of grinding and polishing. One slice of this quenched sample, the single-annealed diffusion multiple (1200 °C–500 h), did not undergo any further annealing and is labeled sample #1. The second and third slices of the 1200 °C–500 h annealed diffusion multiple underwent grinding and encapsulation in the argon-filled quartz tubes, were heat treated at 800 °C for 1000 h and 700 °C for 1000 h, respectively, and then water quenched to ambient temperature; these are labeled sample #3 and sample #4.

The other whole diffusion multiple was encapsulated in a quartz tube and first annealed at 1200 °C for 500 h, then quenched to ambient water. It was then re-encapsulated (without being sliced into disks) in a quartz tube and heat treated at 900 °C for another 500 h. The diffusion multiple was then quenched to ambient water, sectioned, ground and polished, and labeled sample #2.

The 1200 °C–500 h first annealing was selected to induce wide composition variations and high solubility in solid-solution phases via long-term interdiffusion. The generation of wide composition gradients is much easier and quicker at a high temperature such as 1200 °C because of the higher diffusivities. For DADM samples, the second heat treatment at an intermediate temperature does not significantly change the average macroscopic composition gradient when compared with the first heat treatment at 1200 °C, and we confirmed this conclusion through diffusion simulations. This is because the diffusivities at intermediate temperatures are orders of magnitude smaller than those at high temperatures. Thus, the composition gradient changes caused by diffusion at the intermediate temperatures are negligible. The second heat treatment at an intermediate temperature is to induce phase precipitation from supersaturated solid solutions. This step is very similar to the annealing of individual alloy samples at a temperature of interest during the phase diagram study or precipitation study of an alloy.

After heat treatment and water quenching, both diffusion multiples were cut parallel to the Ni caps into ~6 mm thick slices by EDM. Specimen slices were polished carefully to observe precipitate morphologies. Scanning electron microscopy (SEM) images were taken to identify different phases with backscatter electron (BSE) imaging and local energy-dispersive spectroscopy (EDS). It is relatively straightforward to identify the phases using BSE and EDS since all the phases are known for the relevant binary systems and the Fe–Cr–Ni ternary system. Electron probe microanalysis (EPMA) was employed for local compositional analysis of the diffusion multiples across phase boundaries/interfaces in order to obtain quantitative compositions of phases as well as to establish the local equilibrium information for tie-lines, and thus to construct the phase diagrams.

The EPMA scan locations were made perpendicular to the interphase interfaces as much as possible (constrained by x – y stage motion of EPMA). It is assumed that interphase interfaces were perpendicular to the polished surface of the diffusion multiples. Effort was made to cut the annealed diffusion multiples in the directly perpendicular to the diffusion directions in cross-sectional plane. Even though two-phase regions are thermodynamically allowed

in ternary systems, they rarely appear in high-temperature (single) annealed diffusion multiples because three elements are diffusing at the same time and this can cause two-phase regions to shrink. When an EPMA beam travels/traverses at a small step size (e.g. 1 μm) along a line across a phase interface, it hits single-phase regions far more often than the two-phase interface and only occasionally hits near or at the interface (thus sampling both phases). Therefore, there are much denser data points from the single-phase regions than from the two-phase regions. The composition–composition Gibbs triangle plots in a form similar to a “diffusion path” show the compositional paths of the scans in the corresponding isothermal section phase diagram. A more detailed description of the diffusion-multiple approach for phase diagram determination as well as ways to analyze the experimental data are provided in Ref. [4], so these are only briefly summarized here. It is the local equilibrium at phase interfaces that defines the tie-lines.

For DADMs at intermediate temperatures, especially the lower bound of the intermediate temperatures, the driving force towards equilibrium is high, but the kinetics/diffusion is slow. Metastable or transient phases/states may emerge, especially during the early stage/time of the annealing. Annealing for extended periods of time (500–1000 h) at intermediate temperatures was used to circumvent this issue. For the Fe–Cr–Ni systems, all the phases observed in the DADM samples are equilibrium phases: bcc, fcc and sigma.

Even for equilibrium phases, when the precipitates are very small, their compositions and the surrounding solid solution compositions interfacing with them can deviate significantly from the equilibrium compositions due to the Gibbs–Thomson effect and other effects. For instance, careful studies using both experimental atom probe tomography and computational lattice kinetic Monte Carlo simulations by Mao et al. [14,15] showed that the supersaturation of both the fcc γ phase and the L_{12} γ' phase of Ni–Cr–Al alloys decreased from about 5–8 at.% to ≤ 0.1 at.% as the annealing time increased from 0.1 to ~1000 h and the average γ' particle size increased from ~1 to ~10 nm. When the precipitate size is greater than 3–5 μm , i.e. large enough for reliable EPMA measurement of its composition, the Gibbs–Thomson effect is minimal and the local equilibrium at the precipitate/matrix (solid solution) interfaces can be assumed. Such local equilibrium assumption for large precipitates is the basis for using equilibrated alloys and diffusion couples for phase diagram determination [4,16]. The equilibrium tie-line compositions reported in the current study were all obtained from such local equilibrium at the interface between a precipitate (>3 μm) and the matrix phase.

Ternary isothermal phase diagrams are established by sorting the information from all tie-lines extracted from EPMA together with the existing information of the binary phase diagrams, such as the solubility and composition ranges of compounds and solution phases. When the composition data acquired by EPMA scans are plotted onto a ternary isothermal section, a straight line connects two single-phase regions outside of which there are dense data points on each side of the single-phase regions; such information greatly helps define tie-lines (see [Supplementary Information](#) and Ref. [4] for more detail). During the process of analyzing EPMA data, it is also very beneficial to plot the composition against the scan distance/location for all points in an individual line scan to form what is

usually called a diffusion profile. Tie-line information can also be extracted from such a diffusion profile by identifying the “jumps” in composition across phase interfaces in the diffusion zone and by extrapolating the local equilibrium compositions to the interface between neighboring phases. By plotting hundreds or thousands of data points from all the line scans onto a Gibbs triangle (isothermal section, i.e. concentration of one element against concentration of another in a triangular plot, with the third concentration being the dependent one, adding to 100% total), a series of tie-lines start to emerge in the ternary isothermal section phase diagram. By correlating the information present in the experimental SEM images, the composition–distance diffusion profile plots, the existing literature, the data point density/distribution and the tie-line alignment, the phase boundaries can be defined for a ternary system. Tie triangles can be drawn designating three-phase regions. As mentioned, knowledge of the binary phase diagrams and the existence of ternary intermetallic compounds is essential information for defining the phase boundaries with certainty.

Unlike analyzing individual alloy samples, where several measurement repeats can be made, every tie-line obtained from a polished cross-section of a ternary system in a diffusion-multiple is the only set of data available. It is the trends and consistency of the neighboring tie-lines obtained from a diffusion-multiple that give confidence to the results.

A typical accelerating voltage (e.g. 15–20 keV) during EPMA excites an interaction volume on the order of a $1\ \mu\text{m}^3$ for relative heavy elements like Fe, Cr and Ni. EPMA scanning is an efficient way to obtain composition profiles with high spatial resolution. The step size and length of the line scans are carefully chosen to balance accuracy, time and budget. All EPMA measurements were performed at a $1\ \mu\text{m}$ step size in this study.

For easy tracking, the four diffusion multiples samples are listed here again: sample #1: 1200 °C–500 h single-anneal; sample #2: 1200 °C–500 h and 900 °C–500 h dual-anneal; sample #3: 1200 °C–500 h and 800 °C–1000 h dual-anneal; and sample #4: 1200 °C–500 h and 700 °C–1000 h dual-anneal. All the experimental results reported in this article were obtained from the Fe–Cr–Ni trijunction location (of the above four samples), as marked by the red square in Fig. 1d.

3. Results and discussion

3.1. 1200 °C Fe–Cr–Ni isothermal section

Sample #1 is a single-anneal diffusion multiple that was heat treated for 500 h at 1200 °C and water quenched to ambient temperature. The only stable phases in the Fe–Cr–Ni ternary system at 1200 °C are α and γ , and they coexist over a wide composition range. Fig. 2 is an SEM BSE image of the Fe–Cr–Ni trijunction area in sample #1. The interphase interface between α and γ , separating the two phases, with γ on the top and α at the bottom (the contrast between Cr and Fe is due to the sharp composition gradient near pure Cr rather than a phase transition) can be clearly seen. EPMA was performed across the γ/α interface to obtain composition profiles (see line scans 2, 3 and 4, as marked in Fig. 2).

Based on the EPMA results, an isothermal section of the Fe–Cr–Ni ternary system at 1200 °C is obtained. The phase boundary and tie-lines can be easily defined for such a simple

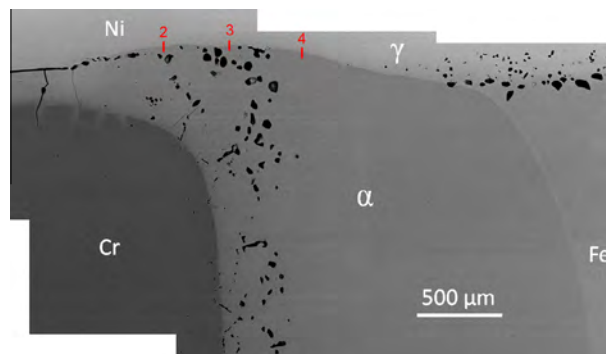


Fig. 2. SEM image showing the γ and α phases and their interface in the Fe–Cr–Ni tri-junction of the single-anneal diffusion multiple that was annealed at 1200 °C for 500 h (sample #1).

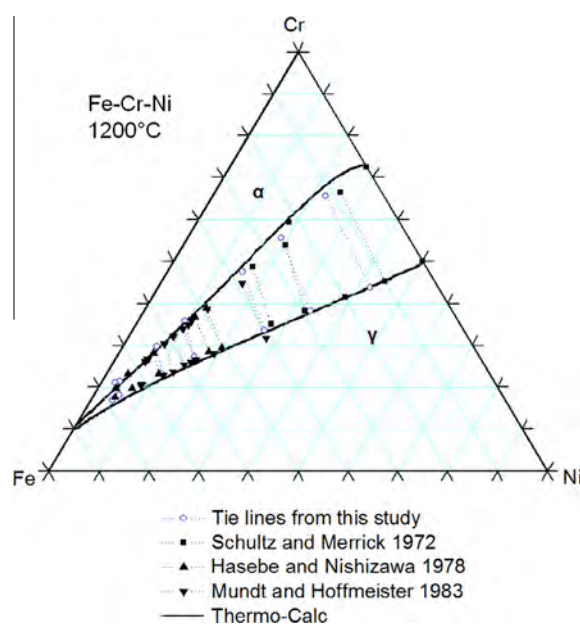


Fig. 3. Tie-lines of the 1200 °C Fe–Cr–Ni isothermal section (plotted in at.%, with the axis numbers removed for simplicity) determined from this study in comparison with other experimental results reported in the literature [7,8,10] superimposed on the calculated isothermal section using Thermo-Calc [17,18] and the TCFE5 thermodynamic database.

system. The extracted tie-lines are plotted in Fig. 3 in comparison with all the available experimental tie-line data from the literature [7,8,10], as well as the computed 1200 °C isothermal section using Thermo-Calc [17,18] and the TCFE5 thermodynamic database. The agreement among all the experimental data sets is excellent. The calculated Ni solubility in the Cr-rich α phase is slightly lower than the experimental measurements, but the overall agreement between the experimental data and the calculation result is excellent at this temperature.

Note that no precipitates were observed in sample #1 (Fig. 2), which was quenched directly from 1200 °C, indicating that water quenching allows the high-temperature γ and α phases to be retained to room temperature without decomposition. The result clearly shows that the massive α to σ transformation that will be described subsequently did not take place during quenching. This information is very

useful in understanding the σ phase transformation mechanism later.

3.2. 900 °C Fe–Cr–Ni isothermal section and phase transformations

Sample #2 is a DADM which was first annealed at 1200 °C for 500 h and then annealed again at 900 °C for another 500 h. By performing EPMA line scans across the interfaces between large precipitate phases and the surrounding matrix phases, the ternary Fe–Cr–Ni isothermal section at 900 °C was established.

Fig. 4 is an SEM montage image of the trijunction region of sample #2. The α/γ interface formed at the 1200 °C heat treatment can still be identified from the dashed red line superimposed on the image (note the regions above and below this line were single-phase γ and α before the 900 °C annealing). There are densely populated precipitates with different morphologies on both sides of the initial α/γ interface (dashed red line). SEM images of the four small boxed areas in Fig. 4 are shown in Fig. 5 (labeled a–d). Fig. 5a is from the Cr-rich area, showing fine needle-like γ precipitates in the α matrix below the dashed line and coarser α precipitates in the γ matrix above the

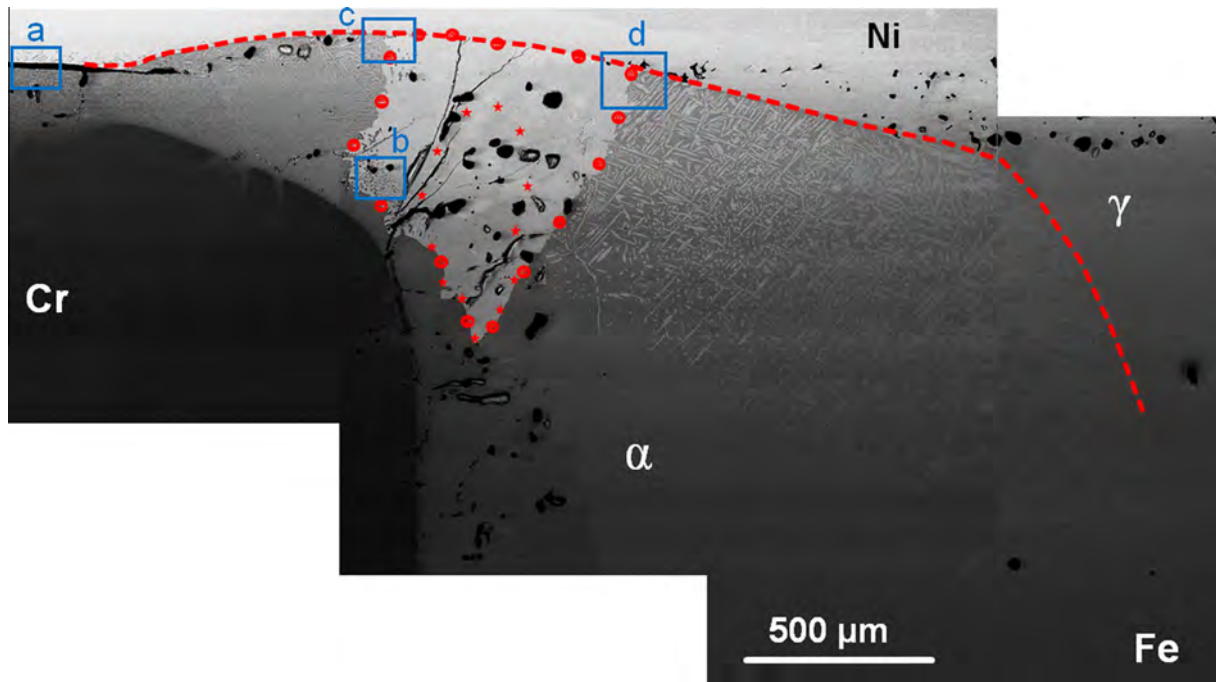


Fig. 4. SEM image montage showing the overall phase distribution of the Fe–Cr–Ni trijunction in sample #2 (1200 °C for 500 h + 900 °C for 500 h).

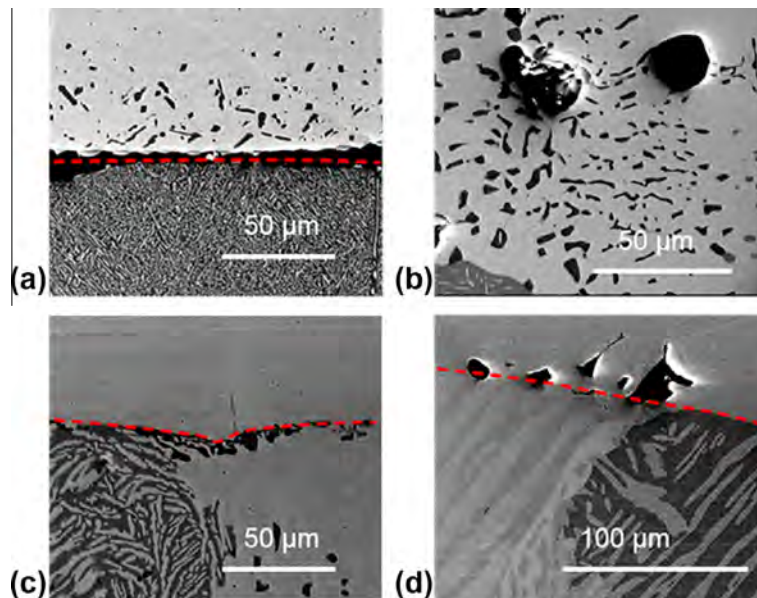


Fig. 5. SEM images showing precipitates in sample #2. The locations are marked in Fig. 4.

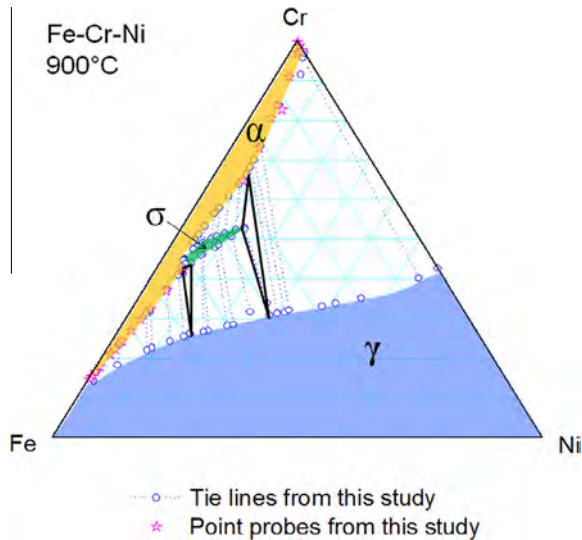


Fig. 6. The 900 °C Fe–Cr–Ni isothermal section determined from a DADM (sample #2). The phase diagram is plotted in at.%, with the axis numbers removed for simplicity.

dashed line. Fig. 5b shows α precipitates (dark) from the σ matrix and the lower left corner of this image captured a few needle-like γ precipitates in the α matrix. Fig. 5c shows the γ phase at the top, the σ phase at the lower right (with α precipitates) and the γ precipitates in the α matrix at the lower left. Fig. 5d is from the Fe-rich side and shows the γ phase at the top, the γ precipitates in the α matrix at the lower right and the long streaky γ precipitates in the σ matrix at the lower left. Many of the precipitates in Figs. 4 and 5 are large enough to allow EPMA line scans

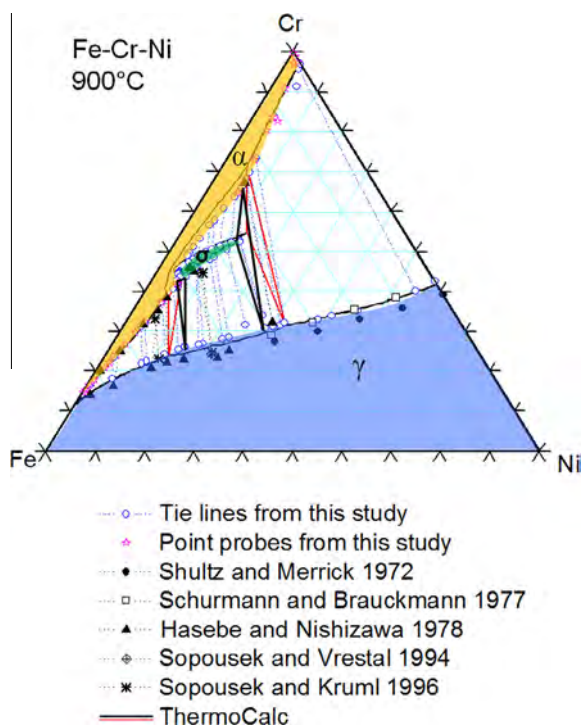


Fig. 7. The 900 °C Fe–Cr–Ni isothermal section (at.%) determined from this study in comparison with prior experimental data from the literature [4–6,8,9] as well as the Thermo-Calc calculation result.

to be performed across the precipitate/matrix interfaces to extract tie-lines.

Fig. 6 shows the 900 °C isothermal section of the Fe–Cr–Ni ternary phase diagram established from a series of tie-lines obtained from EPMA scans across many precipitate/matrix interfaces. The open circles are tie-lines extracted from local equilibrium between the precipitate phases and the matrix phases, and the stars are results of EPMA point analysis along the locations separating the precipitate-containing and precipitate-free regions. Point probes were performed in the α matrix along the edges of γ precipitates. The data are shown as stars in Fig. 6 and they help define the single-phase boundary of the α phase. The results of the EPMA point analyses and the tie-line extractions are in good agreement, and together they define the α phase boundary well.

Fig. 7 compares the 900 °C Fe–Cr–Ni isothermal section determined from the current study with prior experimental data from the literature as well as the Thermo-Calc calculation result. The Cr solubility in the γ phase obtained from the current study is in good agreement with the result reported by Schurmann and Brauckmann [9], and is about 1–3 at.% higher than the data reported by other groups [7,8,11,12]. The Ni solubility in the α phase in equilibrium with the γ phase agrees well with the reported values from the literature in the Fe-rich side; and the current study provided new data on the Cr-rich side. The current study provides experimental data on the solubility of Ni in the α phase in equilibrium with the σ phase for the first time, and the result indicates that Thermo-Calc slightly underpredicts this solubility.

As shown in Fig. 7, the tie-lines obtained from the current study show the same trend as the experimental results reported in the literature, suggesting that the two $\alpha + \sigma + \gamma$ three-phase triangles computed by Thermo-Calc may not be very accurate, especially concerning the γ phase compositions in the $\alpha + \sigma + \gamma$ three-phase equilibria.

The results presented in Figs. 6 and 7 show that a complete and reliable 900 °C isothermal section of the Fe–Cr–Ni system was very effectively obtained from a single DADM (sample #2). The same amount of experimental data would otherwise require many individual alloys to be made, annealed for extended period of time and then analyzed one at a time.

Massive transformation is a composition-invariant and thermally activated transformation which involves short-range diffusion and associated interface migration [19–21]. It is postulated that the bright area in the middle of Fig. 4 enveloped by the red dots underwent a massive α to σ transformation during the initial stage of heat treatment at 900 °C. It is noted that such transformation did not occur during quenching of the 1200 °C annealed sample to ambient temperature since no σ phase was present in sample #1 (Fig. 2). Parts of the σ phase formed through the composition-invariant massive transformation during the initial 900 °C annealing are supersaturated with respect to the 900 °C phase diagram/solubility. During further extended annealing (for 500 h) at 900 °C, the supersaturated parts decomposed to precipitate the α phase in some of the left-hand area of the σ matrix (Figs. 4 and 5b and c) and to precipitate the γ phase in some of the right-hand side and top area of the σ matrix (Figs. 4 and 5d). Only the area demarcated by the small red stars remained as single-phase σ , corresponding to the direct α to σ massive transformation from single phase to single phase without

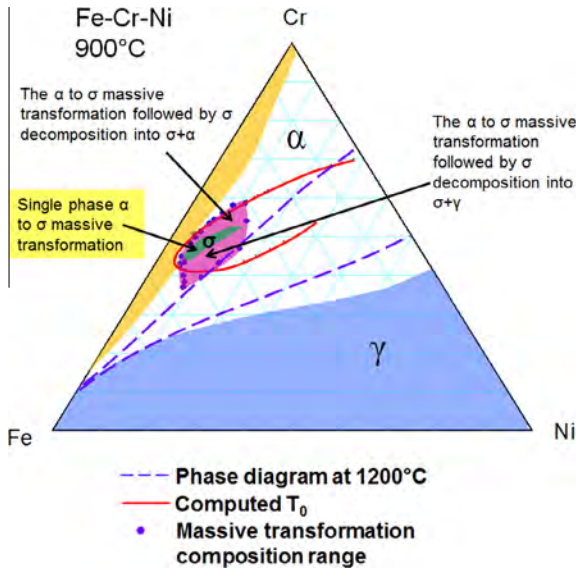


Fig. 8. Explanation of the α to σ massive transformation taking place during isothermal annealing at 900 °C and the subsequent decomposition of parts of the massive σ during the extended annealing at 900 °C for 500 h. See text for details.

decomposition even after extended annealing at 900 °C. The above hypothesis can be better understood with the help of Fig. 8, which combines the experimental measurements with thermodynamic calculations that predict the T_0 line at which compositions the Gibbs energy of the α phase is equal to that of the σ phase at 900 °C. Inside this T_0 envelope, the Gibbs free energy of the α phase is higher than that of the σ phase, thus the α to σ massive transformation is thermodynamically possible. To test whether the bright area in the middle of Fig. 4 enveloped by the red dots satisfies the thermodynamic condition, EPMA point analysis

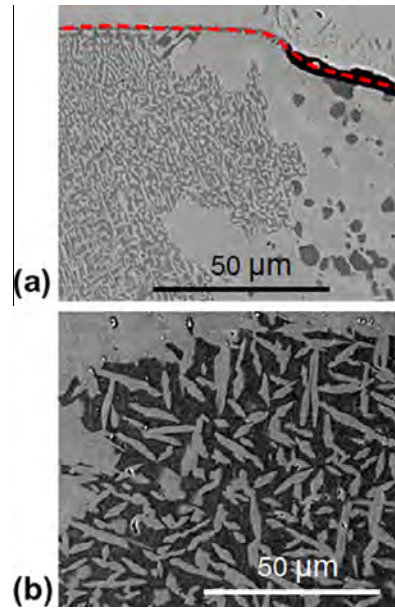


Fig. 10. SEM images showing precipitates in the Fe–Cr–Ni region of sample #3.

was performed on the areas of the red dots and the compositions are shown in Fig. 8. It can be seen that the measured compositions (blue dots) are mostly within the T_0 envelope (only a few data points are outside, which could be due to the inaccuracy of the thermodynamic parameters). Both the morphology and the thermodynamic analysis support the hypothesis that the bright area in the middle of Fig. 4 underwent the α to σ massive transformation during the early stage annealing at 900 °C. The α to σ massive transformation has clearly taken place in some two-phase regions of the 900 °C phase diagram (Fig. 8), supporting

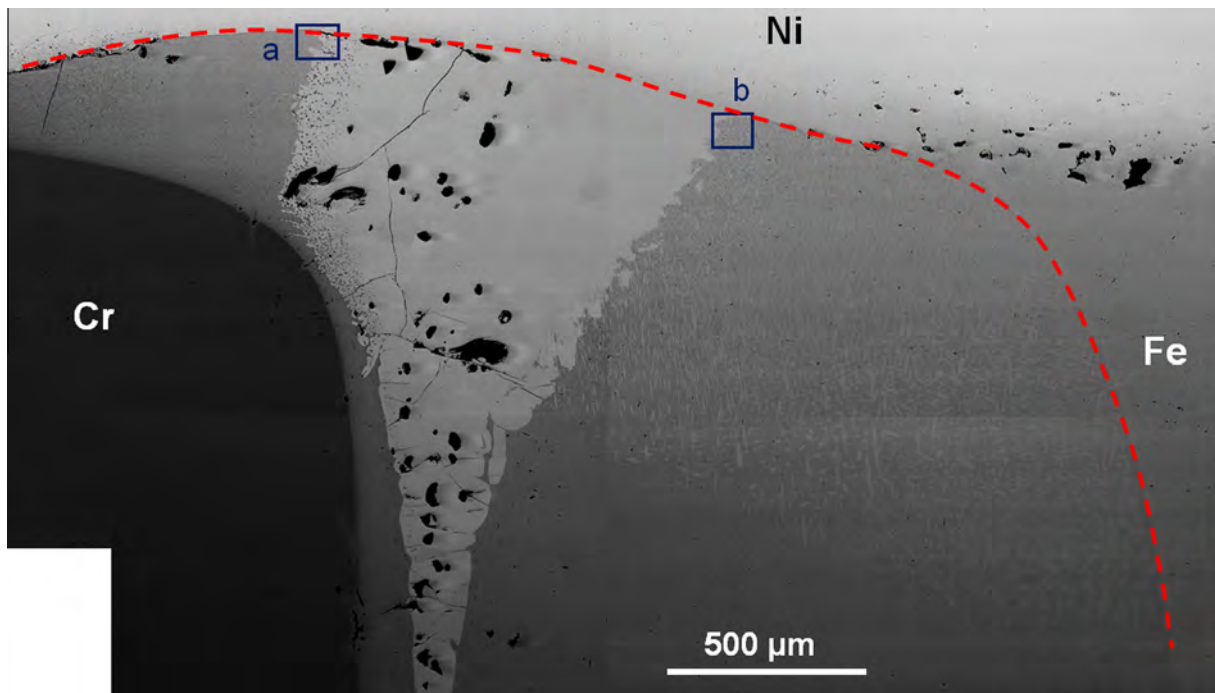


Fig. 9. SEM image montage showing the distribution of phases in the Fe–Cr–Ni trijunction region of sample #3 (1200 °C–500 h + 800 °C–1000 h).

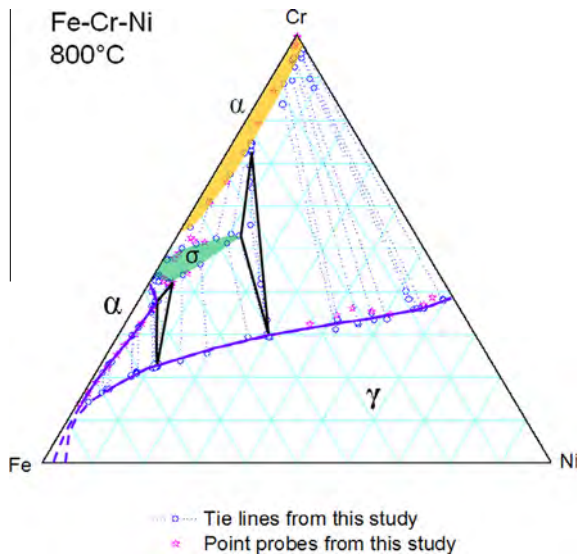


Fig. 11. The 800 °C Fe–Cr–Ni isothermal section determined from this study using a DADM (sample #3). The phase diagram is plotted in at.%, with the axis numbers removed for simplicity.

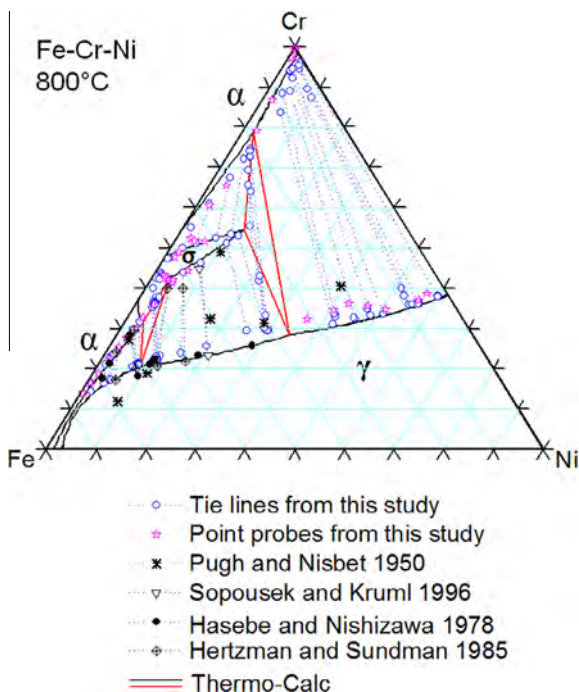


Fig. 12. The 800 °C Fe–Cr–Ni isothermal section (at.%) determined from this study in comparison with the Thermo-Calc calculation result as well as prior experimental results reported in the literature [8,12,13,22].

Hillert's assertion that such an occurrence is possible [21]. After extended (500 h) annealing at 900 °C, the σ phase formed by massive transformation but with its composition inside the two-phase regions of the 900 °C isotherm would decompose to precipitate the second phase in the σ matrix to reach the respective two-phase equilibrium, as shown in Fig. 8. Such a precipitation phenomenon was observed in the SEM images in Figs. 4 and 5.

One can imagine that such systematic information on the phase transformation mechanism of the σ phase would be hard to obtain from studies on individually made alloys unless a large number of alloys are made near the σ phase region. Such work would be very time-consuming and costly to perform, and thus has never been done/reported.

There is rich information on the precipitate morphology in Figs. 4 and 5 as a result of the nucleation and growth of precipitates across a wide range of different compositions. Sample #2 (Fig. 4) itself serves as a rich atlas of precipitation microstructures for the Fe–Cr–Ni system, and can be used to check the computation simulation results of this system. Future detailed work on the sample could provide more detailed information on the transformation kinetics of the system.

3.3. 800 °C Fe–Cr–Ni isothermal section and phase transformations

Sample #3 is a DADM that was annealed at 1200 °C for 500 h and then annealed at 800 °C for another 1000 h. Fig. 9 is an SEM montage image of the ternary phase region, with the original γ/α interface formed at the 1200 °C marked with a dashed red line. The bright area in the middle is the σ phase matrix, which is presumably formed through a massive transformation in a similar fashion to that described for sample #2 (Figs. 4 and 8).

Fig. 10 presents two higher-magnification SEM images, taken from the Cr-rich and Fe-rich sides of the σ phase region (marked as boxes a and b in Fig. 9, respectively). These show the α precipitation from the σ matrix (bright) in Fig. 10a and the γ precipitates in the α matrix (dark) in Fig. 10b. By performing a detailed EPMA analysis in a way similar to that demonstrated for sample #2, large amounts of equilibrium phase diagram information were obtained from sample #3 to construct the 800 °C isothermal section of the Fe–Cr–Ni ternary system, as shown in Fig. 11.

The precipitates in sample #3 (Figs. 9 and 10) are very similar to those in sample #2 (Figs. 4 and 5) but at much finer scales, due to the lower temperature of the second annealing for sample #3. Fig. 9 once again provides a rich atlas of precipitate morphology that was induced by the various phase transformations taking place in the different compositions during precipitation annealing at 800 °C.

Fig. 12 compares the result obtained from the current study with the experimental results from the literature as well as the result computed using Thermo-Calc. There is overall agreement on the general topology of the phase diagram, but some differences can be noted. For instance, the Cr solubility in the γ phase obtained from the current study is about 2–3 at.% higher than most data reported by prior studies, except those reported by Pugh and Nisbet [22], which are quite different from all other data sets.

Similar to the scenario in Fig. 7, the tie-lines obtained from the current study, presented in Fig. 12, show the same trend as most of the experimental results reported in the literature, suggesting that the two $\alpha + \sigma + \gamma$ three-phase triangles computed from Thermo-Calc may not be very accurate, especially concerning the γ phase compositions in the $\alpha + \sigma + \gamma$ three-phase equilibria.

3.4. 700 °C Fe–Cr–Ni isothermal section and phase transformations

Sample #4 is a DADM that was first annealed at 1200 °C for 500 h and then at 700 °C for another 1000 h. Fig. 13 is an SEM BSE image montage showing the overall phase distribution in the Fe–Cr–Ni trijunction. Some of the details of the precipitates are shown at higher magnification in Fig. 14. Fig. 14a shows long α precipitates in the γ matrix in the top part and the very fine γ precipitates in the α matrix at the bottom. Fig. 14c shows very dense γ precipitates in the Cr-rich α matrix on the left and the α precipitates in the σ matrix on the right. Fig. 14b shows γ precipitates in Fe-rich α matrix in the lower right corner and the γ precipitates from the σ matrix at the lower left.

An isothermal section of the Fe–Cr–Ni system at 700 °C (Fig. 15) has been constructed based on EPMA measurements of sample #4. The σ phase boundary is relatively well defined, but the $\gamma + \sigma + \alpha$ (Cr-rich) three-phase equilibrium is not well defined based on the existing data. Difficulty was encountered in EPMA scans of γ precipitates in the α matrix as some of the particles are too small for reliable EPMA of single-phase compositions.

Fig. 16 compares the experimental results from the current study with those reported in the literature, as well as computed results using Thermo-Calc and TCFE5 database. It can be clearly seen that the thermodynamic calculation has predicted a composition region of the σ phase at 700 °C that is much smaller than the experimental observations, and the solubility of Cr in the γ phase is significantly higher than that calculated by Thermo-Calc. The results from sample #4 are in reasonable agreement with those of Hertzman and Sundman [13], except for the $\gamma + \sigma + \alpha$ three-phase triangle for which appreciable difference is observed.

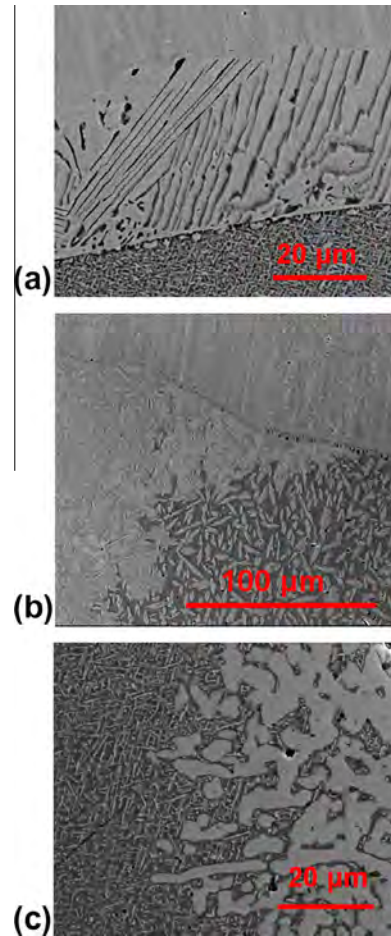


Fig. 14. SEM images showing precipitates in the Fe–Cr–Ni trijunction of sample #4. The locations are marked in Fig. 13.

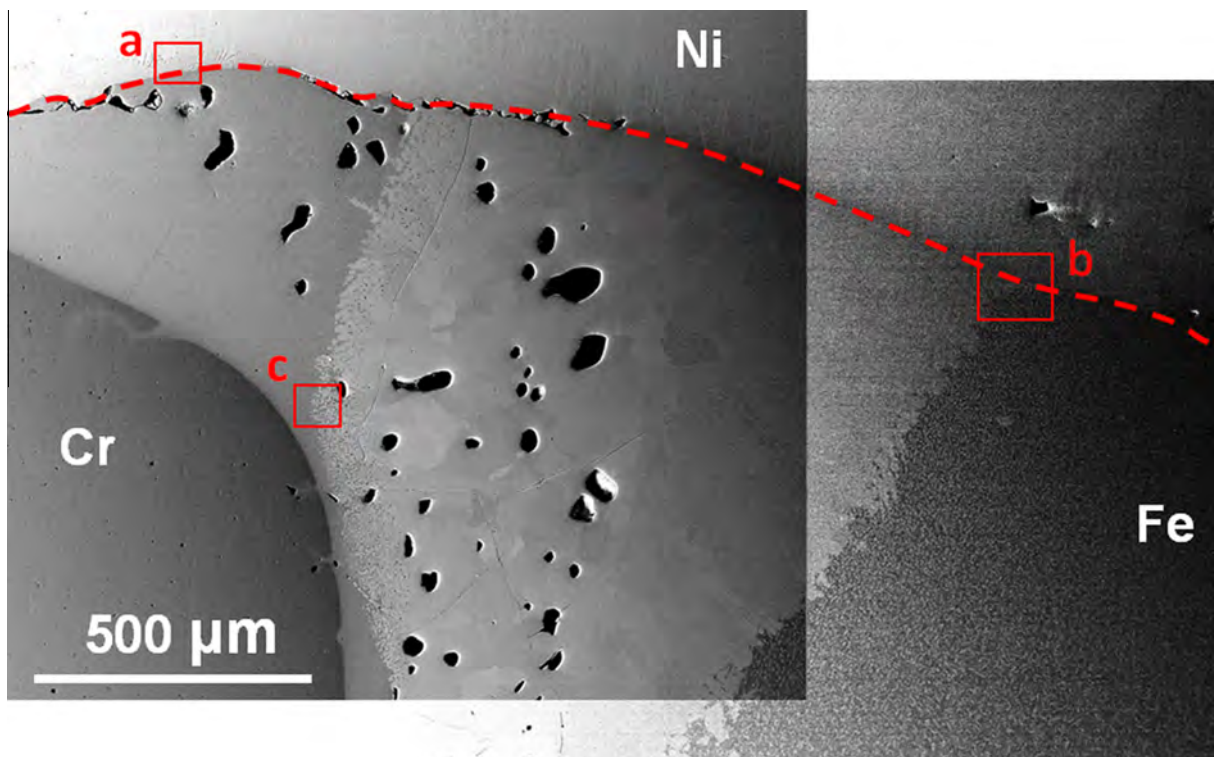


Fig. 13. SEM image montage showing the overall phase distribution in the Fe–Cr–Ni trijunction of sample #4 (1200 °C–500 h + 700 °C–1000 h).

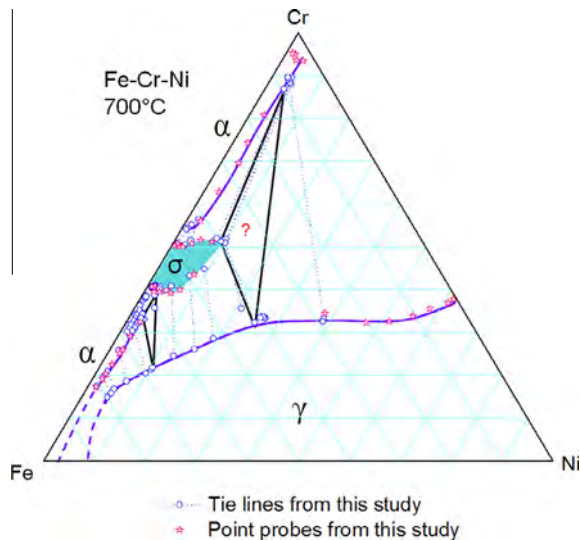


Fig. 15. Tentative 700 °C isothermal section of the Fe–Cr–Ni system determined from this study. The phase diagram is plotted in at.%, with the axis numbers removed for simplicity.

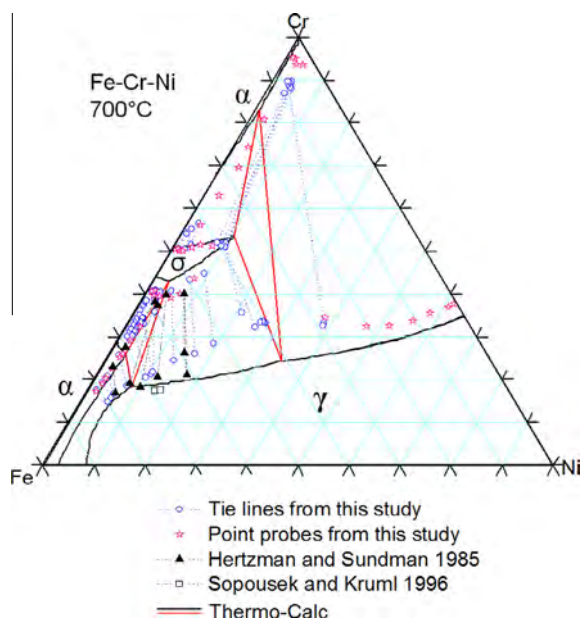


Fig. 16. The 700 °C Fe–Cr–Ni isothermal section (at.%) determined from this study in comparison with the Thermo-Calc calculation result as well as experimental results reported in the literature [12,13].

4. Summary and conclusions

A DADM approach was tested for the effective determination of intermediate-temperature phase diagrams, as well as the effective study of phase transformations. One 1200 °C (500 h) single-anneal diffusion multiple and three DADMs were made and analyzed to study the phase equilibria of the Fe–Cr–Ni system at 1200, 900, 800 and 700 °C, as well as the associated phase transformations. Tie-lines were obtained from EPMA data by taking advantage of the local equilibrium at the interphase interfaces. EPMA point analysis was also used to pinpoint the single-phase boundaries along which the precipitate-free zones were separated from precipitate-laden zones. The results from tie-

line analysis and EPMA single-point analysis are in good general agreement. Reliable isothermal sections at 1200, 900 and 800 °C were obtained; and the large amount of new data collected from the DADMs will be very valuable for improving the thermodynamic assessment of the Fe–Cr–Ni system. At lower temperatures such as 700 °C, even after being annealed for 1000 h, some of the precipitates are too small to allow reliable EPMA tie-line evaluation in certain composition regions of the phase diagram. The results obtained for the 700 °C isothermal sections are obtained only from those precipitates that are large enough and thus are somewhat incomplete. Careful transmission electron microscopy EDS quantitative analysis would be required to construct reliable and complete isothermal sections at temperatures lower than 700 °C for the Fe–Cr–Ni system.

Our analysis of the morphology/microstructure and composition of the σ phase matrix formed in DADMs, together with the calculation of the T_0 lines, strongly suggests that the σ phase was initially formed through massive transformation during the early stage of the second isothermal annealing. Prolonged annealing induced the precipitation of α and γ phases for the σ phase composition regions that sit in two-phase fields at the second temperature.

The Fe–Cr–Ni isothermal sections at 1200, 900 and 800 °C obtained from diffusion multiples in this study agree with the majority of prior experimental measurements reported in the literature. This supports the reliability of the DADM approach in the determination of phase diagrams at intermediate temperatures. The much higher efficiency of the DADM approach is clearly demonstrated for the Fe–Cr–Ni ternary system.

A very diverse collection of precipitate morphologies and microstructures (Figs. 4, 5, 9, 10, 13 and 14) was obtained from the Fe–Cr–Ni trijunction of the three DADMs, and provides valuable experimental data to validate computational simulation results in the future. The diverse microstructures and consistency as a result of compositional variation can be clearly seen in each montage image (Figs. 4, 9 and 13), and the refinement of α precipitates as a function of decreasing precipitation annealing temperature can be clearly seen (Fig. 4 vs. Fig. 9 vs. Fig. 13), even though sample #3 (800 °C) and sample #4 (700 °C) were annealed for 1000 h instead of 500 h, as in the case of sample #2 (900 °C).

The microstructures (Figs. 4, 9 and 13) obtained in this study are the results of nucleation, growth and coarsening, since the precipitation annealing was performed for extended periods of time (500 or 1000 h). To systematically study the nucleation process as a function of composition variation and/or temperature, one could perform more, but shorter precipitation anneals.

The wide atlases of microstructure could help identify trends of phase transformation. For instance, we deduced the mechanism of α to σ phase transformation to be massive transformation in nature. We can also quickly see whether a precipitate emerges with a spherical morphology or as other shapes, such as plates or needles. Such morphological information could help us to understand the roles that lattice strain and interfacial energy may play in dictating the precipitation and growth of a particular phase.

It is our dream that researchers will be able to simulate the entire range of morphological variants in a DADM across the entire composition range to reproduce the observed microstructures using phase field or other methods in conjunction with thermodynamic and kinetic databases.

An agreement between the simulation and experiments would provide strong validation of the simulations. Agreement in certain areas and disagreement in other areas of the same DADM sample may provide clues for the improvement of the simulation methodologies, mechanisms or data.

Acknowledgements

The authors would like to thank Dr. John Donovan and Ms. Julie Chouinard for their help in the microprobe analysis performed at the CAMCOR Facilities of the University of Oregon. This study was performed at The Ohio State University with support from the National Science Foundation (NSF) of the United States under Grant number DMR-1237577. Part of the microprobe analysis was financially supported by the Outokumpu Corporation. The diffusion multiple sample components were machined and provided by the Carpenter Technology Corporation.

Appendix A. Supplementary data

Supplementary data associated with this article can be found, in the online version, at <http://dx.doi.org/10.1016/j.actamat.2014.12.027>.

References

- [1] J.-C. Zhao, *Adv. Eng. Mater.* 3 (2001) 143.
- [2] J.-C. Zhao, *J. Mater. Sci.* 39 (2004) 3913.
- [3] J.-C. Zhao, *Prog. Mater. Sci.* 51 (2006) 557.
- [4] J.-C. Zhao, in: J.-C. Zhao (Ed.), *Methods for Phase Diagram Determination*, Elsevier Ltd, Oxford, 2007, p. 246.
- [5] E.C. Bain, W.E. Griffiths, *Trans. AIME* 75 (1927) 166.
- [6] F. Wever, W. Jellinghaus, *Mitt. Kaiser-Wilhelm-Inst. Eisenforsch. Dusseldorf.* 13 (1931) 93.
- [7] J.W. Schultz, H.F. Merrick, *Metall. Trans.* 3 (1972) 2479.
- [8] M. Hasebe, T. Nishizawa, in: G.C. Carter (Ed.), *NBS Special Publication No. 496. Applications of Phase Diagrams in Metallurgy and Ceramics, Vol. 2*, NBS, Gaithersburg, MD, 1978, p. 911.
- [9] E. Schurmann, J. Brauckmann, *Arch. Eisenhuettenwes* 48 (1977) 3.
- [10] R. Mundt, H. Hoffmeister, *Arch. Eisen.* 54 (1983) 253.
- [11] J. Sopousek, J. Vrestal, *Z. Metallkd.* 85 (1994) 111.
- [12] J. Sopousek, T. Kruml, *Scr. Mater.* 35 (1996) 689.
- [13] S. Hertzman, B. Sundman, *Scand. J. Metall.* 14 (1985) 94.
- [14] Z. Mao, C. Booth-Morrison, C.K. Sudbrack, G. Martin, D.N. Seidman, *Acta Mater.* 60 (2012) 1871.
- [15] Z. Mao, C.K. Sudbrack, K.E. Yoon, G. Martin, D.N. Seidman, *Nat. Mater.* 6 (2007) 210.
- [16] F.J.J. van Loo, *Prog. Solid State Chem.* 20 (1990) 47.
- [17] B. Sundman, B. Jansson, J.-O. Andersson, *CALPHAD* 9 (1985) 153.
- [18] J.-O. Andersson, T. Helander, L. Höglund, P. Shi, B. Sundman, *CALPHAD* 26 (2002) 273.
- [19] T.B. Massalski, *Phase Transformations*, ASM, Metals Park, OH, 1970, p. 433.
- [20] T.B. Massalski, *Metall. Mater. Trans. A* 33 (2002) 2277.
- [21] M. Hillert, *Phase Equilibria, Phase Diagrams and Phase Transformations: A Thermodynamic Basis*, Cambridge University Press, Cambridge, 1998.
- [22] J.W. Pugh, J.D. Nisbet, *J. Met.* 188 (1950) 268.